Indeed, the slope of this variation and the isopycnic point are very different for proteins, lipids, nucleic acids, *etc.*, thus allowing the determination of the chemical composition, including solvent, of each region.

X-ray small-angle scattering is a good tool for the determination of the overall shape and size of globular particles whatever their internal structure, because the small molecules used to change the contrast are unlikely to penetrate the particle and do not give rise to additional internal-density fluctuations. Neutron scattering in $^1H_2O/^2H_2O$ buffers covering a large range of contrasts, on the other hand, provides a unique possibility to get an insight into the internal organization of complex biological particles (see also Luzzati, Tardieu, Sardet, Le Maire, Osborne & Chabre, 1983).

I thank especially Dr B. Jacrot, European Molecular Biology Laboratory Outstation, Grenoble, and Dr A. Tardieu, Centre de Génétique Moléculaire, Gif-sur-Yvette, for stimulating discussions.

References

BENOIT, H. & WIPPLER, C. (1960). *J. Chim. Phys.* **57**, 524–527.
BRAGG, W. L. & PERUTZ, M. F. (1952). *Acta Cryst.* **5**, 277–283.
CHARLES, M., SÉMÉRIVA, M. & CHABRE, M. (1980). *J. Mol. Biol.* **139**, 297–317.
CHAUVIN, C., PFEIFFER, P., WITZ, J. & JACROT, B. (1978). *Virology*, **88**, 138–148.
GUINIER, A. (1939). *C. R. Acad. Sci.* **208**, 894–896.
IBEL. K. & STUHRMANN, H. B. (1975). *J. Mol. Biol.* **93**, 255–265.
JACROT, B. (1976). *Rep. Prog. Phys.* **39**, 911–953.
JACROT, B. (1981). *Comprehensive Virology*, Vol. 17, edited by H. FRAENKEL-CONRAT & R. WAGNER, pp. 129–182. New York: Plenum Press.
JACROT, B., CHAUVIN, C. & WITZ, J. (1977). *Nature (London)*, **266**, 417–421.
LEE, B. & RICHARDS, F. M. (1971). *J. Mol. Biol.* **55**, 379–400.
LE MAIRE, M., MOLLER, J. V. & TARDIEU, A. (1981). *J. Mol. Biol.* **150**, 273–296.
LUZZATI, V. & TARDIEU, A. (1980). *Ann. Rev. Biophys. Bioeng.* **9**, 1–29.
LUZZATI, V., TARDIEU, A. & AGGERBECK, L. A. (1979). *J. Mol. Biol.* **131**, 435–473.
LUZZATI, V., TARDIEU, A., SARDET, C., LE MAIRE, M., OSBORNE, H. B. & CHABRE, M. (1983). *Structure, Dynamics, Interactions and Evolution of Biological Macromolecules*, edited by C. HÉLÈNE, pp. 283–298. Dordrecht, Holland: Reidel.
LUZZATI, V., WITZ, J. & NICOLAÏEFF, A. (1961). *J. Mol. Biol.* **3**, 367–378.
SARDET, C., TARDIEU, A. & LUZZATI, V. (1976). *J. Mol. Biol.* **105**, 385–407.
STUHRMAN, H. B., HAAS, J., IBEL, K., KOCH, M. H. J. & CHRICHTON, R. R. (1976). *J. Mol. Biol.* **100**, 399–413.
STUHRMAN, H. B. & KIRSTE, R. G. (1965). *Z. Phys. Chem. (Frankfurt am Main)*, **46**, 247–250.

Acta Cryst. (1983). A**39**, 711–718

The Experimental Determination of the Phases of X-ray Reflections*

BY BEN POST

Physics Department, Polytechnic Institute of New York, 333 Jay Street, Brooklyn, New York 11201, USA

(*Received* 25 *October* 1982; *accepted* 11 *April* 1983)

Abstract

The application of dynamical diffraction theory to the 'phase problem' for centric crystals shows that the intensities diffracted in simultaneous three-beam interactions display characteristic maxima and minima. The sequence in which these appear on chart recordings is a sensitive function of the phase of the triplet involved in the interaction. The sequence is the same for all triplet phases of the same sign; it is reversed for those of the opposite sign. In earlier work a number of triplet phases in perfect crystals were determined. In the present work, several hundred triplet phases in mosaic crystals have been determined. Details of one of these investigations are reported in the following paper [Gong & Post (1983). *Acta Cryst.* A**39**, 719–724].

* This work was supported by the National Science Foundation and by the Joint Services Electronics Program of the Defense Department.

0108-7673/83/050711-08$01.50

Introduction

In previous publications (Post, 1977, 1979), it was shown that the spatial distribution of the intensity diffracted by a centrosymmetric crystal in n-beam simultaneous diffraction ($n > 2$) is a sensitive function of the invariant phase of the structure-factor triplet involved in the interaction. This indicated that the signs of such phases could be retrieved directly from the diffracted intensities. Some success was finally achieved and several examples of experimental phase determination were included in the works cited above. These were based on photographic recordings of intensities transmitted through perfect and slightly imperfect thin crystals of germanium and aluminum oxide.

A major objective of the present work involves the demonstration that similar phase effects may be displayed in n-beam diffraction by *mosaic* crystals, comparable in quality, or lack of it, to crystals commonly used in crystal structure investigations. This

has been done. The signs of several hundred triplet phases in centrosymmetric mosaic crystals of zinc tungstate,* lead molybdate and sulfamic acid have been determined from their n-beam patterns. Detailed descriptions of one of these investigations are given in the following paper (Gong & Post, 1983).†

Examples of intensities recorded in n-beam diffraction involving three and four beams are given in Figs. 1 and 2. Analysis of the patterns, based on considerations which were discussed briefly in the 1977 and 1979 papers, and which are dealt with more fully in this manuscript, shows that the triplet phases of the interactions in Fig. 1(*a*) and (*b*) are positive and those in Figs. 2(*a*) and (*b*) are negative. The description of the procedures used to arrive at these conclusions presupposes some familiarity with the dynamical diffraction theory of Ewald (1917). A discussion of selected elements of the theory which are considered to be relevant to the 'phase problem' is therefore included in the sections immediately following. The phase-determination procedure and related matters are then discussed.

Chart recordings of simultaneous n-beam diffraction patterns display characteristic maxima and minima about n-beam settings. The experimental determination of triplet phases is based on the analysis of the sequences in which those intensity asymmetries appear on the charts. We have observed large numbers of intensity asymmetries, similar to those shown in Figs. 1 and 2, in n-beam patterns of *perfect and mosaic* crystals. We have been unable to account for either the characteristic shapes of the interactions, or their relationships to triplet phases, on the basis of conventional kinematical considerations. As we will show below, both those aspects of n-beam interactions are accounted for satisfactorily when the problem is treated by the methods of dynamical diffraction.

It is well known that diffraction by mosaic crystals involves incoherent interactions among optically independent perfect domains as well as coherent inter-

* The author is indebted to Dr William Roth, of the National Bureau of Standards, for providing the zinc tungstate and various other crystals for this investigation.

† Preliminary results were presented at the Spring, 1982 meeting of the American Crystallographic Association at the National Bureau of Standards, by P. P. Gong, J. A. Nicolosi & B. Post.

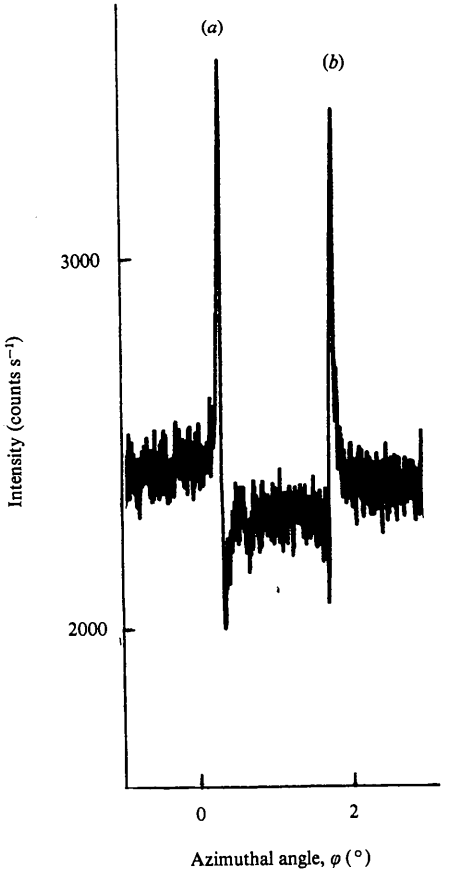

Fig. 1. Small portion of a simultaneous diffraction pattern of zinc tungstate. Cu $K\alpha_1$ radiation.

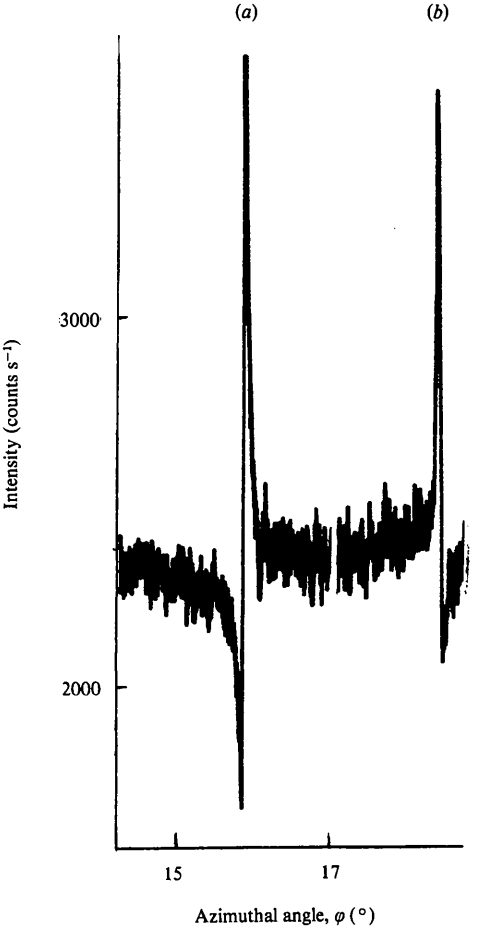

Fig. 2. Further small portion of a simultaneous diffraction pattern of zinc tungstate. Cu $K\alpha_1$ radiation.

actions within those domains. The former include 'secondary extinction' effects. They often constitute major fractions of the total recorded intensity in two-beam diffraction. They play a less important role in n-beam diffraction ($n > 2$).

In order to generate incoherent n beam diffraction it is necessary that 'n' independent domains be aligned critically relative to one another. In addition, the divergence of the incident beam is generally reduced, in properly conducted n-beam experiments, to values much smaller than those normally used in two-beam diffraction, in order to resolve the intensity asymmetries under discussion. The combination of the above greatly reduces the likelihood that incoherent n-beam interactions will occur frequently enough to affect the phase indications significantly.

Variations of the sizes of coherent domains may generate more serious difficulties. It will be shown below that the intensity asymmetries are due largely to selective absorption effects within coherent domains. They are relatively unimportant in small domains, *i.e.* in those with small values of μt; these scatter X-rays kinematically and contribute mainly to the general background.

The phase-determining asymmetries appear to be due mainly to the relatively small numbers of 'large' domains in the crystal. In our work to date only from 5 to 10% of the possible interactions yield useful phase indications.

The experimental data are produced by the interaction of an incident beam, whose divergence, even after reduction, is large in dynamical terms, with a crystal whose mosaic spread and anisotropy are generally unknown. It is clearly very difficult to achieve quantitative evaluations of the data. Fortunately, the experimental determination of triplet phases involves essentially qualitative procedures which are relatively insensitive to the aberations mentioned above.

There appears to be little to be gained from separate discussions of dynamical effects in perfect and mosaic crystals. Our treatment is therefore more general. Modifications of the analysis should be made to suit individual cases.

I. Theory

(*A*) *The fundamental equation*

The kinematical theory of diffraction provides the theoretical basis for crystal structure investigations which utilize conventional two-beam diffraction. Its many approximations and omissions, however, render it unsuited for the detailed analysis of n-beam simultaneous diffraction needed for experimental phase determination. For the latter we make use of the self-consistent theory of Ewald (1917), as modified by Laue (1931). Useful discussions of the theory are available (Ewald, 1969; James, 1963; Batterman & Cole, 1964).

Laue has shown that the calculation of n-beam dynamical diffraction effects involves the solution of Maxwell's equations for a medium with a periodic complex dielectric constant, under conditions which satisfy Bragg's Law. A sum of plane waves is taken as the assumed solution for the wavefields in the crystal:

$$\mathbf{D} = \sum_H \mathbf{D}_H \exp - (2\pi i \mathbf{K}_H . \mathbf{r}). \qquad (1)$$

$\mathbf{K}_H$ is a wave vector in the crystal, with magnitude $1/\lambda$(cr), directed to the reciprocal-lattice point (r.l.p.) indicated by its subscript; $\mathbf{D}_H$ is the corresponding electric displacement vector; $\mathbf{r}$ is a vector in the surface of the crystal. $\mathbf{K}$ is the vacuum wave vector; its magnitude is $1/\lambda$(vac).

Using Bragg's law, ($\mathbf{K}_H = \mathbf{K}_0 + \mathbf{H}$), we have:

$$\mathbf{D} = \exp - (2\pi i \mathbf{K}_0 . \mathbf{r}) \sum_H \mathbf{D}_H \exp -(2\pi i \mathbf{H} . \mathbf{r}). \qquad (2)$$

The solutions of Maxwell's equations lead to a set of linear homogeneous equations for the amplitudes:

$$\mathbf{D}_H = -\frac{\Gamma}{2\varepsilon_H} \sum_L F_{(H-L)}\, \mathbf{D}_{L[H]}. \qquad (3)$$

H and L are r.l.p.'s; $\mathbf{D}_{L[H]}$ is the vector component of $\mathbf{D}_L$ which is perpendicular to $\mathbf{K}_H$. $\Gamma = e^2\lambda^2/4\pi^2\varepsilon_V mc^2 V$; V is the volume of the unit cell; ε_V is the permittivity of vacuum; other terms have their usual meanings. $\Gamma = 1{\cdot}175 \times 10^{-7}$ for Cu $K\alpha$ and a cell volume of 180 Å^3. ε_H is a negative quantity which serves as a measure of the deviation from geometrical diffraction conditions. A detailed derivation of (3) is given in Appendix *A* of Batterman & Cole (1964).

Equation (3) is the fundamental equation of dynamical diffraction. It was first derived by Ewald in 1917. The summation on the right is nominally taken over all r.l.p.'s but, because most terms have negligible magnitudes, it is limited in practice to a few large terms, *i.e.* to terms whose ε_H's are very small. The corresponding r.l.p.'s are then considered to be in their 'diffracting positions'. The number of terms in the summation is generally the same as in the equivalent kinematical calculation.

(*B*) *The number of equations*

Equation (3) yields n vector equations for n-beam diffraction. To deal with polarization, each $\mathbf{D}_H$ is usually decomposed into two mutually perpendicular components to form $2n$ scalar equations, *i.e.* six equations for three-beam cases. The permitted values of the ε_0's are the solutions of the secular determinant of (3). In most cases, especially at small Bragg angles, these solutions occur in the form of pairs of ε_0's with

similar values. The small differences are due to polarization effects. To reduce mathematical difficulties, without significant loss of accuracy, those differences will be ignored, leaving only n scalar equations.

(C) *The dispersion surface (DS)*

The DS is the locus in reciprocal space of the solutions of (3); the ε_H's, scaled by multiplication by k, are plotted as functions of the azimuthal angle of crystal rotation. In Fig. 3, $\mathbf{k}$ and $\mathbf{K}_0$ are drawn from the origin of the reciprocal lattice towards C, the center of the sphere of reflection. $\mathbf{k}$ terminates at C; $\mathbf{K}_0$ ends just short of it. Magnitudes are greatly distorted in the figure. R, the radius of the sphere, $= |\mathbf{k}| = 6{\cdot}49 \times 10^7$ cm^{-1}. The difference between the lengths of $\mathbf{K}_0$ and $\mathbf{k}$ is of the order of a few hundred cm^{-1}, or about $R \times 10^{-5}$. Points 1, 2, 3 are marked along $\mathbf{K}_0$ to represent its terminus for each of three solutions of (3).

The large arc through C represents a small portion of a section through the 'Laue sphere', $R = |\mathbf{k}|$; the second arc does the same for the 'Lorentz sphere', $R' = \langle|\mathbf{K}_0|\rangle$, the reciprocal of the average wavelength within the crystal.

The positions of ε_0 and of all r.l.p.'s are fixed when the orientation of $\mathbf{K}_0$ is fixed, and they change when the latter changes. Once ε_0 is determined, using (3), all the ε_H's can be calculated from geometry (Hildebrandt, 1967). Changes in the orientation of $\mathbf{K}_0$, due, say, to the divergence of the incident beam, cause points 1,2 and 3 to sweep out small areas, the 'sheets' of the DS.

The DS is the sum of all the sheets. It displays graphically most of the significant features of the diffraction process. Relevant boundary conditions are taken into account by drawing inward normals, originating at points on the surface on which the incident beam impinges. The intersections of each inward normal with the sheets are the 'tiepoints' for the corresponding crystal setting (see Figs. 4 and 5).

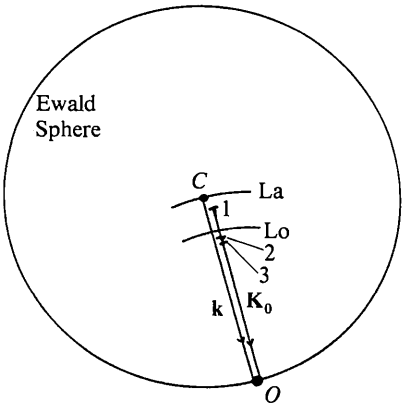

Fig. 3. Wave vectors in reciprocal space. $\mathbf{K}_0$ and $\mathbf{k}$ originate at O and are parallel to one another.

Additional sets of tiepoints are generated as the crystal is rotated. The surface boundary conditions as well as Maxwell's equations are satisfied at the tiepoints, each of which serves as the source of wave vectors directed to the r.l.p.'s involved in the interaction.

(1) *The one-beam DS (no diffracted beams).* For this case the solution of (3) is trivial. Only D_0 need be considered. We have

$$\varepsilon_o^{(1)}\mathbf{D}_0 = -(\Gamma/2)F_0\mathbf{D}_0. \tag{4}$$

The superscript refers to n, the number of beams. The one-beam DS is a spherical shell (the Lorentz shell). Its radius, $|\mathbf{K}_0|$, $= k(1 + \varepsilon_0)$. $k\varepsilon_0$ equals the difference between the radii of the Lorentz shell and the slightly larger Laue shell. The ratio of the radii, $|\mathbf{K}_H|/k$, equals the average refractive index of the crystal for the radiation used. It is of the order of $1{-}10^{-5}$ for most materials if Cu $K\alpha$ is used.

(2) *The two-beam DS.* The coefficients of the $\mathbf{D}$'s for the exact two-beam settings may be arranged in a 2×2 determinant (for the simplified DS). On expansion, this gives (Post, 1979)

$$|F_H|^2 = \pm|(F_0 + 2\varepsilon_0/\Gamma)|^2. \tag{5}$$

Both sides of (5) consist of squared terms. Ewald (1968) has pointed out that this makes it impossible to determine phases directly from two-beam diffraction data.

It is useful to rewrite (5) to show F_H as an explicit function of ε_0, *i.e.*

$$\left(\frac{k\Gamma}{2}\right)F_H = \pm\left[\left(\frac{k\Gamma}{2}\right)F_0 + k\varepsilon_0^{(2)}\right]. \tag{6}$$

In the plane of the paper the two-beam DS consists of two lines symmetrically disposed about the Lorentz 'line'. The distances from the sheets to the latter are equal and proportional to F_H. At the Lorentz line $F_H = 0$, φ is the azimuthal angle, the angle of rotation about

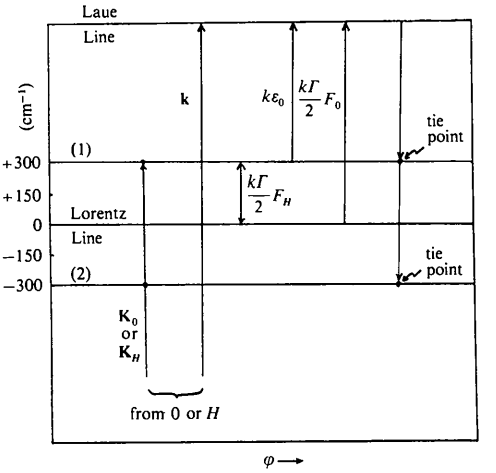

Fig. 4. The two-beam dispersion surface.

the diffraction vector; it equals zero at the exact three-beam settings (Fig. 4).

(3) *The three-beam DS.* Unlike the two-beam DS, which is invariant to changes in φ for constant Bragg θ, the conditions for three-beam diffraction are satisfied only at discrete values of φ. At exact three-beam settings the DS, in the plane of the paper, consists of three points, the solutions of (3). In Fig. 5 these coincide with the intersections of the DS sheets and the vertical line at $\varphi = 0$. The Lorentz point, Lo, is the origin of the coordinate system.

For $\varphi = 0$, expansion of the determinant of the coefficients of the D's yields a cubic equation of the form:

$$X^3 + AX + B = 0, \tag{7}$$

$$X = \left(F_0 + \frac{2\varepsilon_0^{(3)}}{\Gamma}\right); \quad A = -\sum_i^2 |F_i|^2;$$

$$B = 2F_H F_L F_{(L-H)}.$$

The roots (R_i) of (7) are calculated by standard methods:

$$R_i = \mp 2(-A/3)^{1/2}\,[\cos(\Phi + Y_i)], \quad i = 1, 2, 3; \tag{8}$$

$$Y_i = 0, 120, 240°; \quad \Phi = \frac{1}{3}\cos^{-1}\left(-\frac{B^2}{4}\frac{27}{A^3}\right)^{1/2}.$$

Because of the absence from (7) of any term quadratic in X, the sum of the roots equals zero. In general, there will be three real unequal roots. The *signs* of the roots, but not their magnitudes, are functions of the sign of the invariant triplet phase, *i.e.* the sign of B. The minus symbol in (8) signifies that the sign of the largest root is the negative of that of B. The signs of the smaller roots are the same as that of B.

The magnitudes of two of the roots are larger than those of any of the F's involved in the triplet. The third root is smaller than any of the F's. Because the sum of the roots must equal zero, only one of the large roots lies between the Lorentz and Laue lines. One three-beam root is closer to the Laue line than either two-beam sheet, for positive *and* negative phases. To approximate the two- to three-beam transition regions of the DS the two-beam sheets should be joined smoothly to the points which represent the roots at $\varphi = 0$. The transition regions in Figs. 5(*a*) and (*b*) were sketched in that way. Two sets of F's, with identical absolute values, but differing in their triplet phases, were used to calculate the two- and three-beam roots. Note that Fig. 5(*b*) is related to 5(*a*) by a 180° rotation about the Lorentz line. That is expected. A change in the sign of the triplet phase implies a corresponding change in the signs of the three roots.

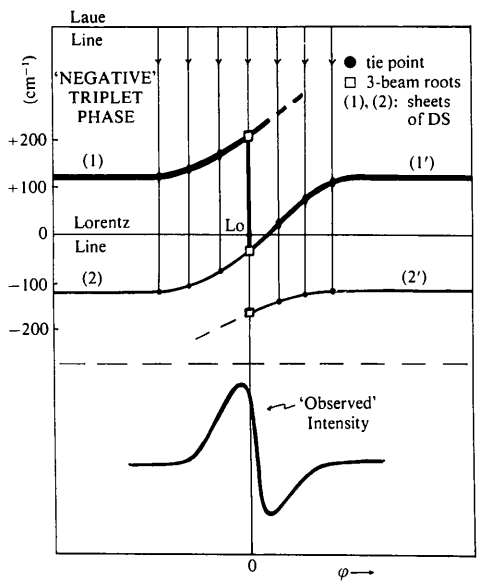

(*a*)

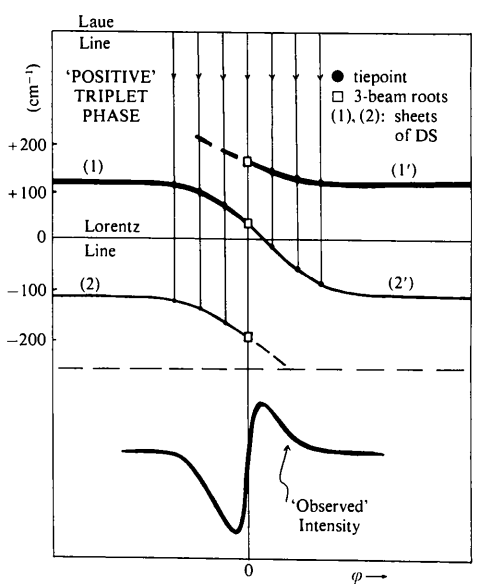

(*b*)

Fig. 5. The three-beam dispersion surface, showing transitions from two to three beams, *i.e.* from an interaction involving 0 and H to one involving 0, H and L.

(*D*) *Absorption*

Ewald (1968) has shown that absorption coefficients approach zero near the Laue line and increase with increasing separation from that line. They reach μ_0 at the Lorentz line and continue to increase beyond that. μ_0 is constant for a given crystal and wavelength. It is equal to the average of all the coefficients at any crystal setting.

In two-beam diffraction the absorption coefficients of the sheets differ, but each maintains a constant value as long as only two beams are involved. In regions of transition from two to three beams, the coefficients of sheets change with changing distance from the Laue line.

(*E*) *n-beam peak profiles*

It is evident that most of the diffracted intensity which emerges from a crystal is due to diffracted waves which originate at tiepoints on the sheets nearest the Laue line. That effect is enhanced in regions near three-beam settings. For positive and negative phases only one of the two largest roots lies between the Lorentz and Laue lines. Two-beam sheets approach three-beam lines from both sides. One sheet must curve upward in order to be joined to the three-beam root, as is shown in Figs. 5(*a*) and (*b*). This results in a further decrease in the already low absorption coefficients together with an increase in the observed intensity.

It is useful to examine Fig. 5(*a*) in terms of changing φ; *i.e.* by moving across the figure from left to right. At the extreme left, normal two-beam diffraction prevails. Closer to the three-beam settings, sheet 1 begins to curve upward, as noted above. The intensity rises above its normal two-beam value, reaching a maximum near the three-beam line. Crossing that line is equivalent to the passage of the secondary r.l.p., *L*, through the surface of the Ewald sphere. To the right of the three-beam line, the excitations of the tiepoints on sheet 1 drop rapidly to zero. Away from the surface of the sphere, r.l.p. *L* soon reverts to its original status as a one-beam case.

Additional surface normals are generated to the right of the three-beam boundary; they pass through three sheets in that region but only the lower two need be taken into account. To the right of the three-beam line, sheet 2 becomes the source of tiepoints with the lowest absorption coefficients. Those are larger than the sheet 1 coefficients. The intensity decreases to values lower than the normal two-beam values. Further to the right, sheet 2 moves upward across the Lorentz line to become sheet 1′ on the right; the intensity increases correspondingly until it reaches its two-beam value.

The Fig. 5(*a*) triplet phase is labelled 'negative'. The DS for 'positive' phase is shown in Fig. 5(*b*). There, comparable movement from left to right produces, first, an intensity decrease, then a sharp rise to a maximum value, and, finally, a gradual return to the two-beam value.

The peak profiles shown below Figs. 5(*a*) and (*b*) represent estimates of the intensity distributions expected for the two cases. The intensities and the left–right symmetries differ. The former is of minor importance for phase determination. The latter provides the means of distinguishing positive from negative triplet phases.

II. Experimental

(*A*) *n-beam intensities*

Clearly, the sequences of maxima and minima on strip-chart recordings of *n*-beam interactions can be reversed if the direction of crystal rotation is reversed. Similarly, the corresponding sequence displayed when a r.l.p. enters the Ewald sphere will be reversed when that r.l.p. leaves the sphere, as shown in Fig. 6. The effect of such a reversal resembles the effect produced by changing the sign of a triplet phase. This point has also been noted by Chang (1981).

Difficulties caused by that similarity can be readily eliminated. The distinction between r.l.p.'s entering the Ewald sphere and those leaving is made routinely in calculating the azimuthal angles at which *n*-beam interactions occur (Cole, Chambers & Dunn, 1962). The invariant phases of three-beam interactions, whose patterns show asymmetries of the types discussed, can then be placed in one of the two categories available to centrosymmetric crystals. Positive and negative phases will then be grouped separately.

(*B*) *Absolute phases*

In discussing the procedure for joining two-beam sheets to three-beam roots, we neglected to point out that there are two distinct ways in which that could be done, for positive or negative phases. Either type of intensity asymmetry could equally well have been designated as 'positive', or 'negative'. At present we have no valid grounds for selecting one in preference to the other. The phase assignments, as shown in Fig. 5, for example, are arbitrary. Their arbitrary character can be eliminated by determining one invariant phase independently, by statistical or other methods. It then becomes possible to assign correct absolute triplet phases to all the three-beam interactions in question.

(*C*) *The Renninger method*

A slightly modified version of the Renninger experimental arrangement (Renninger, 1937) has been used

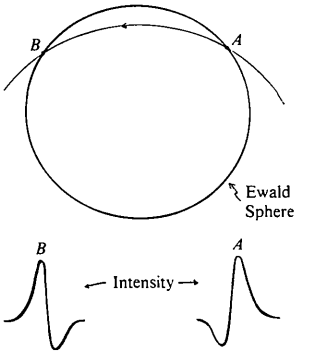

Fig. 6. Intensity profile sequences for reciprocal-lattice points entering and leaving the Ewald sphere.

in our laboratory for several years to collect n-beam diffraction data. The Renninger method is well suited for systematic and rapid recording of n-beam diffraction patterns, and avoids many difficulties inherent in transmission methods, particularly those related to absorption.

There are significant differences between the Renninger and the Bragg methods. The latter generally involves a scan over an angular range in the plane of incidence. The reflection maximum under study is usually near the center of the Bragg range. In the Renninger arrangement, the crystal is first fixed at the exact Bragg angle. It is then rotated about the diffraction vector without disturbing the θ setting.

Rotation of the crystal about the diffraction vector results in the passage of large numbers of secondary reflections successively through widely scattered points on the surface of the Ewald sphere. To achieve adequate resolution under those conditions, it is desirable to reduce the divergence of the incident beam by approximately equal amounts in all directions in the beam cross section. This incident beam divergence causes the saturation of the DS to be spread over a large angular range. Kato (1958) showed that '...the direction of energy flow corresponding to a tiepoint on a particular sheet of the DS is that of the normal to the surface at that point'. There is general agreement on the above (Ewald, 1968; Batterman & Cole, 1964). The properties associated with a tiepoint are independent of the methods used to select or excite the tiepoint. Thus, the conclusions drawn from Fig. 5 regarding three-beam interactions studied by reflection methods should not be affected significantly by the fact that the figure was originally prepared to illustrate a transmission experiment, provided that a substantial region of the DS was saturated by the incident beam.

(D) *'Bragg' angles*

In two-beam diffraction, the angle between $\mathbf{K}_0$ and the perpendicular bisector of the diffraction vector, $\mathbf{H}$, is the two-beam Bragg angle. A similar relation holds in three-beam diffraction.

When r.l.p.'s 0, H and L are simultaneously in their diffracting positions, a line from the center of the Ewald sphere, normal to the plane of the $0HL$ triangle, passes through the midpoint of the latter and is inclined to the propagation vectors $\mathbf{K}_0$, $\mathbf{K}_H$ and $\mathbf{K}_L$ by equal amounts. We label the two angles θ_2 and θ_3 (Fig. 7).

θ_3 is encountered explicitly in one- to three-beam transitions. The $0HL$ plane of Fig. 8 is rotated, as shown, into the Ewald sphere. The circular intersection increases in size with increasing tilt angle. When D touches the surface of the Ewald sphere, the conditions for three-beam diffraction are satisfied. The tilt angle equals θ_3. It is larger than the two-beam Bragg angles that can be formed with any of the three vectors, $\mathbf{H}$, $\mathbf{L}$, or $\mathbf{L} - \mathbf{H}$.

In Renninger diffraction, the angle between $\mathbf{K}_0$ and the primary diffracting planes does not vary. In the small angular interval in which three-beam diffraction takes place, that two-beam angle becomes irrelevant;

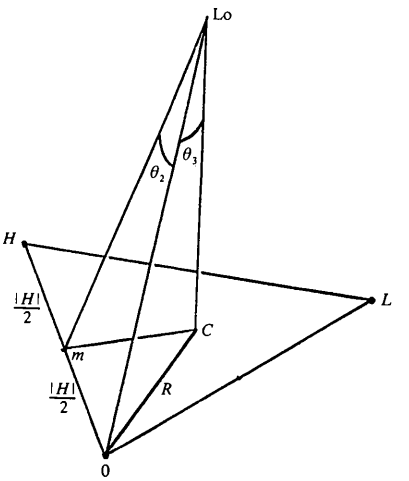

Fig. 7. Two-beam (θ_2) and three-beam (θ_3) diffraction angles.

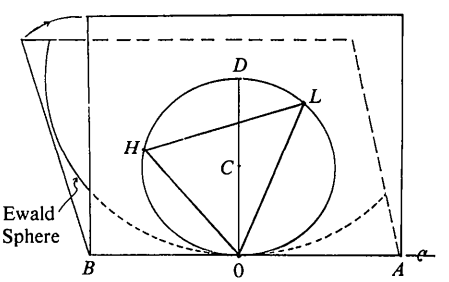

Fig. 8. One-beam to three-beam transition.

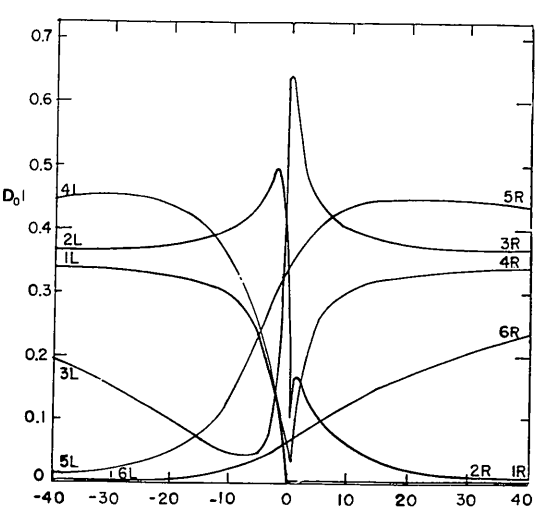

Fig. 9. Effects of a two- to three-beam transition on field amplitudes.

the relevant angle is then θ_3. The change in diffraction angles, from θ_2 to θ_3, leads to sudden changes in beam polarizations. The effects of the latter on the amplitudes of the $\mathbf{D}_0$'s are illustrated in Fig. 9; all six sheets of the three-beam DS were taken into account to calculate the figure. The amplitudes, which are stable in two-beam regions, change by large amounts near the exact three-beam setting, owing to the shift in diffraction angle. In most cases, these amplitude and polarization-angle changes are restricted to regions within about 30 to 40″ of the three-beam setting. Note that the amplitudes of two of the modes decrease to negligible values outside those regions, leaving four modes for the two-beam regions, as expected.

Fig. 9 and similar calculations that we have made for many three-beam cases show that it is very difficult to make meaningful measurements of three-beam intensities near the exact three-beam line, unless the divergence of the incident beam can be restricted to about 1 or 2″, which is difficult to do at present. They also indicate that measurements of regions outside the 30″ boundary could be physically significant.

The changes in diffraction angle, from θ_2 to θ_3, lead to reductions in atomic scattering factors and increased temperature factors. These should be taken into account in calculating three-beam structure factors.

(*E*) *Aufhellung etc.*

The behavior of the DS in the region of a three-beam interaction shows that *Aufhellung* and *Umweganregung* are simply different aspects of the same phenomenon, and that the two should not be treated separately, as though they represent two distinct types of interactions

(*F*) *General comments*

We believe that the primary objective of an experimental phase-determining procedure should involve the provision of a nucleus of phases, determined with a minimum of ambiguity, to serve as a starting point for the application of direct methods. That may make possible the solution of the probably large numbers of crystal structures which have not been solved using direct methods. In any case, the availability of a starting group of unambiguously determined phases would certainly reduce computing times significantly.

The major problem, of course, involves the determination of the phases of non-centrosymmetric crystals. That, too, is beginning to look promising. There is no reason, in principle, why the methods discussed above should not be applicable to acentric crystals. It would be necessary to replace the qualitative equations which enable us to determine the phases of centric crystals by quantitative measurements of n-beam intensities in stable regions of the DS.

High-intensity sources, longest X-ray wavelengths and new instrumentation, designed specifically for n-beam studies, will undoubtedly be vital factors in the solution of the problems listed above and others that will arise.

References

BATTERMAN, B. W. & COLE, H. (1964). *Rev. Mod. Phys.* **36**, 681–717.

CHANG, S. L. (1981). *Appl. Phys.* A**26**, 221–226.

COLE, H., CHAMBERS, F. W. & DUNN, H. M. (1962). *Acta Cryst.* **15**, 138–144.

EWALD, P. P. (1917). *Ann. Phys. (Leipzig)*, **54**, 519–597.

EWALD, P. P. (1968). *Acta Cryst.* A**24**, 1–15.

EWALD, P. P. (1969). *Acta Cryst.* A**25**, 103–108.

GONG, P. P. & POST, B. (1983). *Acta Cryst.* A**39**, 719–724.

HILDEBRANDT, G. (1967). *Phys. Status Solidi*, **24**, 245–261.

JAMES, R. W. (1963). *Solid State Phys.* **15**, 55–220.

KATO, N. (1958). *Acta Cryst.* **11**, 885–887.

LAUE, M. VON (1931). *Ergeb. Exakt. Naturwiss.* **10**, 133–158.

POST, B. (1977). *Phys. Rev. Lett.* **39**, 760–763.

POST, B. (1979). *Acta Cryst.* A**35**, 17–21.

RENNINGER, H. (1937). *Z. Phys.* **106**, 141–161.